


Stress-induced structural changes in superconducting Nb thin films

Jaeyel Lee¹,^{*}[†] Zuhawn Sung, Akshay A. Murthy,[‡] Anna Grassellino, and Alex Romanenko
*Superconducting Quantum Materials and Systems Center (SQMS), Fermi National Accelerator Laboratory (FNAL),
 Batavia, Illinois 60510, USA*

Nathan S. Sitaraman¹^{*} and Tomás A. Arias
Department of Physics, Cornell University, Ithaca, New York 14853, USA

 (Received 31 March 2023; accepted 7 June 2023; published 27 June 2023)

We report on the analysis of stress-induced structural changes and the formation of an omega (ω) phase in polycrystalline Nb thin films deposited on Si by high-power impulse magnetron sputtering (HiPIMS) for superconducting qubits using x-ray diffraction (XRD), transmission electron microscopy (TEM), and density-functional theory (DFT). XRD analysis indicates that internal stresses in the Nb thin films lead to the formation of $\{112\}\langle 111\rangle$ deformation twins and TEM analysis shows that ω phases nucleate at some of the twin boundaries in the Nb thin films. The size of ω phases ranges from 10 to 100 nm, which is comparable to the coherence length of Nb (≈ 40 nm), and $\approx 1\%$ volume fraction of Nb grains exhibit this ω phase. The details of the formation mechanism and superconducting properties of the ω phases are investigated by DFT and potential roles of the ω phase in Nb as a source of decoherence in superconducting qubits are also discussed.

DOI: [10.1103/PhysRevMaterials.7.L063201](https://doi.org/10.1103/PhysRevMaterials.7.L063201)

Nb thin films have been extensively used for resonators and electrodes of superconducting qubits [1–3]. Scaling up this technology to deliver truly transformational quantum computing solutions to the larger community requires improving metrics such as the coherence times, which represent the period over which information remains in a state of quantum superposition. Specifically, it has been observed that materials defects, such as interfaces, surfaces, and impurities play critical roles in inducing this unwanted quantum decoherence [4–6]. For instance, it has been shown that amorphous regions at various interfaces in the device including metal/air [2,7,8], substrate/air [7,9], and metal/substrate [10,11] act as parasitic two-level systems (TLS) and cause decoherence [12–14]. Similarly, there have been reports on impurities and precipitate formation serving as possible sources of decoherence via pair breaking [3,15]. Identifying the atomistic origins of microwave loss in these devices and mitigating them has rapidly developed into an active research area.

It has been shown that when various pure bcc metals and alloys such as Ta, Ti, and Zr alloys experience stress, this leads to twinning and a subsequent phase transformation from bcc to omega (ω) phase with hexagonal crystal structures [16–18]. There has been a recent report on the formation of ω -phase transition in single crystal Nb when subjected to compressive stress [19,20], but the conditions necessary for this phase transition require further understanding, and the implications for Nb in the thin film geometry remain unclear. As Nb is soft with low yield strength (30–80 MPa) and critical

resolved (20 MPa) shear stress, it is possible that internal stress in Nb thin film is sufficient to induce this metastable phase [21–23]. This topic requires further study, considering the aforementioned low yield strength and the potential for structural changes to hinder superconducting performance as has been observed for the bcc-to- ω phase transition in Nb-Zr alloys [24]. Furthermore, the impact of these changes on electronic and superconducting properties remains unclear.

Here, we report the observation of $\{112\}\langle 111\rangle$ twinning-induced ω -phase formation in Nb thin films for superconducting qubits. We find that this twinning and ω -phase formation in Nb occurs in as-grown Nb thin film on Si, thus indicating internal stress in the Nb thin film is sufficient to induce this phase transformation. Previous XRD analysis shows that Nb thin films are indeed under significant internal stress [25], consistent with a theory of stress-driven twinning and ω phase formation in our as-grown Nb thin films on Si substrate. We use density-functional theory to investigate the formation mechanism for the ω phase and its effect on the superconducting properties of Nb. We also discuss implications of the ω -phase transition for superconducting qubit and superconducting radio-frequency applications.

170 nm thick polycrystalline Nb thin films are deposited on Si (100) substrates at room temperature with a base pressure less than 10^{-8} torr using high power impulse sputtering (HiPIMS) at Rigetti Computing. X-ray diffraction (XRD) analysis is performed on the Nb thin films using Rigaku Smartlab with Cu K α 1 x-ray beam. TEM samples of Nb thin films were prepared by focused ion beam (FIB) with 30 kV Ga⁺ ion beams and damaged layers on the surface of the Nb thin foil are removed using 5 kV and 2 kV Ga⁺ ion beams. High-resolution TEM analysis was performed using JEOL ARM 200 CF microscope with 200 kV electron beam. The

^{*}These authors contributed equally to this work.

[†]jlee406@fnal.gov

[‡]amurthy@fnal.gov

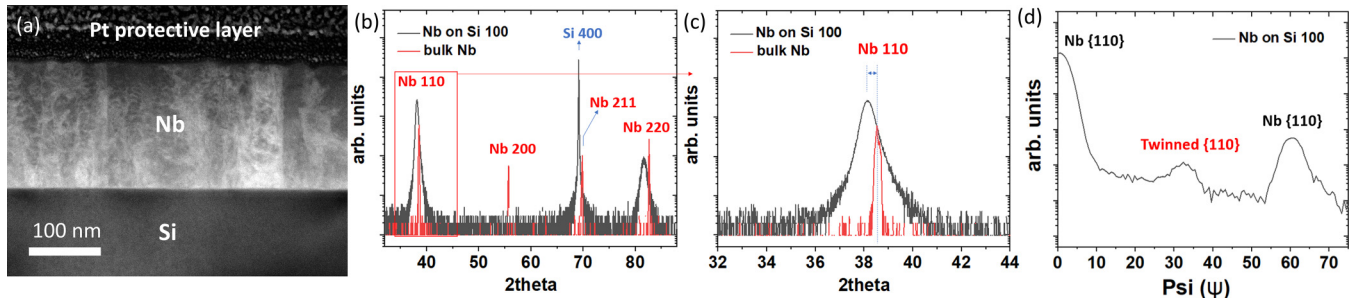


FIG. 1. (a) ADF-STEM image of 170 nm thick Nb thin film on Si (100) substrate deposited by HiPIMS. It shows typical columnar grain structures of Nb thin films on Si substrates for films deposited with this method. (b) X-ray diffraction spectra of the Nb thin film on Si (100) and bulk Nb are displayed. It shows that Nb peaks are shifted toward lower angles from fully relaxed bulk Nb, indicating that Nb thin films are under internal stress. (c) A closer look at the Nb (110) peak shows that Nb (110) peak is shifted to lower angle by 0.5° from relaxed bulk Nb, which corresponds to 1.1% increase of the planar distance of (110) surface normal plane of the Nb thin film on Si (100). (d) Pole figure plot of Nb {110} taken from Nb thin film on Si (100) for a range of ψ values from 0 to 75° displays a Nb {110} peak at $\psi = 0$ and 60° . At $\psi = 33.6^\circ$, we observe an additional peak that arises from twinned {110} parallel to the surface.

microscope was equipped with a Cold FEG source and probe aberration corrector. ADF images were acquired using a convergence semiangle of 21 mrad and collection angles of 68–260 mrad. TEM images are recorded and analyzed using Gatan Micrograph Suite software. Superconducting characterizations using typical four-point electromagnetic characterization is performed in physical property measurement system (PPMS) to estimate the critical temperature and residual resistivity ratio (RRR).

Annular dark-field (ADF)-STEM image of Nb thin film on Si substrate in Fig. 1 displays 170 nm thick Nb thin film on Si (100) substrate. It shows that Nb grains have columnar structures with a 50 nm diameter. XRD spectrum of the Nb thin film on Si (100) is displayed and XRD spectrum of bulk Nb, which is fully relaxed, is also overlaid as a comparison in Figs. 1(b) and 1(c). The XRD spectrum of the Nb thin film demonstrates that the Nb thin film is (110) textured on the Si (100) substrate. Nb (110) peak of the Nb thin film shift to 38.1° compared to bulk Nb from 38.5° , indicating that the surface normal Nb (110) plane of the thin film is expanded by 1.1% due to the in-plane compressive stress in the film. Pole figure of {110} of Nb thin film is taken in Fig. 1(d) and the (110) plane parallel to the surface gives two peaks at $\psi = 0$ and 60° , where ψ is defined as the angle between the surface normal and the diffraction vector. There is an additional peak at $\psi = 34^\circ$, which is likely due to the twinning of the (110) plane parallel to the surface [26]. HR-TEM images of the Nb thin film are provided in Fig. 2 and exhibit the {112}<111> twin, which is also demonstrated by the XRD analysis provided in Fig. 1. We observe it frequently throughout the Nb thin film and it is attributed to the internal stresses in the Nb thin film.

In conjunction with these {112}<111> twins on the surface, we observe the presence of ω -Nb in the surrounding regions. HR-TEM images in Figs. 2(a)–2(c) illustrate the presence of ω -Nb near the surface of the Nb film along with the formation of {112}<111> twins on bcc Nb [1 $\bar{1}$ 0] zone axis. In Fig. 2(b), we observe that bcc Nb and ω -Nb form a sharp interface along the {112}<111> twin boundary. The associated FFT pattern of the HR-TEM images across the ω -Nb and bcc Nb phase in Fig. 2(c) demonstrates the appearance of reflections from

ω -Nb along with the bcc Nb matrix. This satisfies the typical three-dimensional orientation relationships of ω phase in the bcc matrix: $[1\bar{1}0]_{\text{bcc}}//[1\bar{2}10]_{\omega}$ and $(112)_{\text{bcc}}//(\bar{1}010)_{\omega}$ [18,20]. A schematic of the atomic arrangement of Nb atoms of the interface between bcc and ω phase Nb at the twin boundary is illustrated in Fig. 2(d). Further details of the atomic arrangement of the two phases are described in Ref. [20]. The HR-TEM image in Fig. S1 shows that ω -phase transition of Nb also occurs near the Nb/Si interface. In Fig. S1, {112}<111> twin boundary is seen when Nb is tilted to the [113] zone axis and bcc Nb transforms to ω phase across the twin boundary.

In TEM image provided in Fig. 3(a), a lower magnification overview of the morphology of ω phase along the depth-direction of the Nb thin film is illustrated. Here, we observe that the ω phase extends along the entire film thickness (170 nm). A magnified HR-TEM image of the ω phase near the surface on the Nb [113] zone axis is displayed in Fig. 3(b), showing the details of the interface between bcc Nb and ω -phase Nb. The corresponding FFT pattern is provided as an inset and shows the appearance of additional peaks associated with the ω phase. To more clearly illustrate the spatial location of the ω phase, an inverse FFT image using a signal associated only from these additional peaks is provided in Fig. 3(c). We also note that, in a recent report, epitaxially grown single-grain Nb thin films show a lesser amount of internal stress and do not show the ω phase in Nb, and it may imply the possible role of grain boundaries in initiating internal stress-induced {112}<111> twinning and, in turn, ω -phase nucleation at the twin boundaries [27].

From the resistivity measurements (shown in Fig. S3) we observe that this Nb thin film exhibits a critical temperature of 9.3 K with the normal-superconducting transition width ΔT_c ($T_{90\%}-T_{10\%}$) of 0.08 K. The value of residual resistivity ratio (RRR) is estimated to be $\text{RRR} \approx 3.64$ —similar to typical polycrystalline Nb thin films [28]. Due to the limited volume fraction of ω phase (≈ 1 vol.%), physical property measurement system (PPMS) measurements are not well-suited to identify the relationship between this phase and T_c . More detailed characterization of the properties of ω -Nb will require further studies involving specialized geometries and samples.

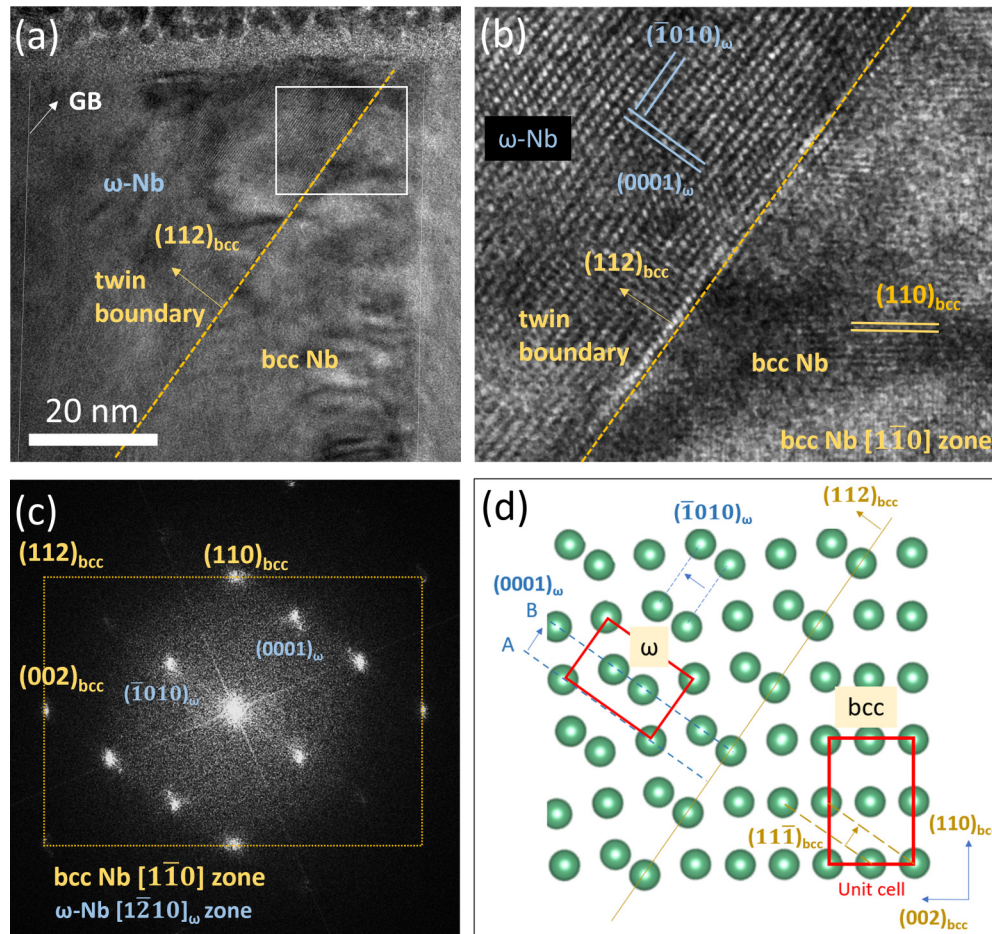


FIG. 2. (a) HR-TEM image of Nb grain on bcc Nb $[1\bar{1}0]$ zone axis with fully transformed ω -Nb phase at $\{112\}\langle 111\rangle$ twin boundary and (b) the details of the twin boundary denoted by the square in Fig. 2(a) are shown. (c) FFT of the HR-TEM image of ω -Nb phase in Nb demonstrates the appearance of reflection from the ω -Nb phase. Three-dimensional orientation relationships (ORs) of ω -Nb phase in Nb are observed, $[1\bar{1}0]_{\text{bcc}}//[1\bar{2}10]_{\omega}$ and $(112)_{\text{bcc}}/(\bar{1}010)_{\omega}$, which is the typical orientation relationships for ω phases in bcc metals. (d) A schematic of atomic structures of the bcc/ ω -Nb interface in Fig. 2(b) is provided. We note that $(0001)_{\omega}$ plane B of ω phase has twice the atomic number density compared to $(0001)_{\omega}$ plane A due to the collapse of two adjacent $(11\bar{1})$ planes from bcc Nb.

Though the ω phase has been widely observed in bcc and hcp metals such as Zr, Ti, and Ta alloys, it has not received significant attention in the case of Nb [29]. As the ω -phase transition has been previously linked to stress [17,19], we consider, in particular, the potential that the ω phases in our thin film are induced by the internal stress in the film, which is also demonstrated by the XRD analysis, Fig. 1. The internal stress is generally seen in sputtered metallic thin films and is caused by various factors such as gas pressures, gas impurities, ion bombardment, and kinetics associated with the growth of thin films during the sputtering process [25,30,31]. Also, we note that the preferred orientation relationships at Nb/Si interface indicated by HR-TEM analysis (Fig. S2), which are in agreement with the previous study, can play a role [7]. Additionally, a high level of O, C, and H impurities near the surface of Nb can cause additional stresses and induce twinning and ω -phase transition [3]. Impurity levels of hydrogen and oxygen in the top surface of Nb is roughly anticipated to be 1–3 at.% [3] and it is predicted to cause 0.2–0.5% of strain on the surface of Nb thin film by lattice expansion. As the Young's modulus of Nb is 104 GPa, the additional stresses caused by impurities in

Nb is 200–500 MPa, which is well above the yield strength and critical resolved shear stress of Nb [32].

To investigate the ω phase in greater detail, we perform density functional theory calculations using the JDFTx density functional theory software package with the PBE exchange-correlation functional and ultrasoft pseudopotentials [33–35]. In particular, we aim to address two key uncertainties about this phase: first, its unexpected stability in Nb despite being much higher energy than the equilibrium bcc phase, and second, its superconducting properties, which have not been investigated yet either experimentally or theoretically.

We find that the omega crystal structure is significantly higher energy than the bcc crystal structure, a difference of 0.31 eV/atom if we assume the ideal lattice relationship $a_{\omega} = \sqrt{2}a_{\text{BCC}}$, $c_{\omega} = \sqrt{3}a_{\text{BCC}}/2$. If allowed to relax, lattice of the ω phase differs significantly from the parent bcc lattice: in particular, we find a 5.6% contraction in the $[111]_{\text{bcc}}//[0001]_{\omega}$ direction, a 4.4% expansion in the $[1\bar{1}0]_{\text{bcc}}//[1\bar{2}10]_{\omega}$ and $[112]_{\text{bcc}}/(\bar{1}010)_{\omega}$ directions, as well as a shear distortion which brings the angle between the $[111]_{\text{bcc}}//[0001]_{\omega}$ and

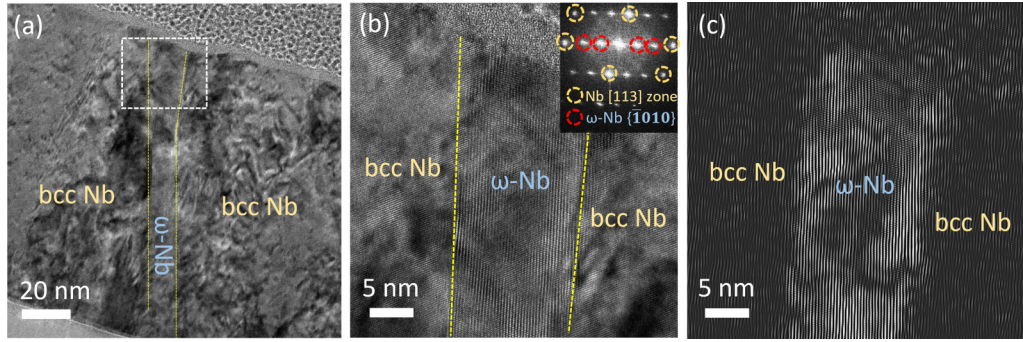


FIG. 3. (a) A low magnification overview of the omega (ω) phase in Nb thin film. (b) A high magnification HR-TEM image of a selected area from the surface to substrate direction in Fig. 3(a). An associated FFT pattern taken from the omega phase is provided as an inset and reflections from bcc Nb [113] zone axis are denoted by yellow dotted circles. Additional reflections from $(\bar{1}010)$ ω -Nb are seen inside the reflections from the bcc Nb on [113] zone axis. (c) Inverse FFT image is taken from the ω -Nb reflections in the FFT of Fig. 3(b) and the morphology of the ω -Nb is displayed.

$[112]_{\text{bcc}}//(\bar{1}010)_{\omega}$ axes to 83° , in agreement with the calculations of Li *et al.* [19]. This relaxation reduces the phase energy difference to 0.20 eV/atom, supporting the idea that stresses could contribute to the bcc-to- ω phase transition.

Whether we take the value of 0.31 eV/atom or 0.20 eV/atom, this is a large phase energy difference. For instance, Li *et al.* [19] finds an energy difference of 0.03 eV/atom for their maximum observed shear strain of 4° . Schnell *et al.* [36] calculated the effect of pressure on phase energy differences in Zr and found a change of about 0.003 eV/(atom \times GPa). Popov *et al.* [37] studied Nb grain boundaries and found an energy of 284 mJ/m² for the $\{112\}\langle 111 \rangle$ twin, equivalent to no more than a single atomic layer of ω phase. Considering these results, we concluded that strain itself may not be sufficient for stabilizing ω phase in bcc Nb. This is in contrast to the case of group 4 elements and group 4–5 alloys in which the energy barriers associated with ω phase formation are generally smaller [38]. Therefore, we consider that other lattice defects, in particular vacancies, are likely to play a role in the stabilization of ω phase in bcc Nb.

We perform calculations on 36-atom bcc and ω supercells to determine the vacancy formation energies in Table I. There is a remarkably large difference in vacancy formation energy between the two phases: the vacancy formation energy in ω phase for sites on $(0001)_{\omega}$ plane B, which is the “collapsed” bcc $(11\bar{1})$ in Fig. 2(c), is negative, indicating that it is energetically favorable for these planes to form with a finite vacancy concentration. The low formation energy of vacancies in ω phase for sites on $(0001)_{\omega}$ plane B and their basic behavior in titanium was previously described by Hennig *et al.* [38]. Therefore vacancies (or dislocations) could play an important role in stabilizing the ω phase, possibly in conjunction with impurities and strain. It also agrees with the observa-

tion that ω phase is likely to nucleate at $\{112\}\langle 111 \rangle$ twin boundaries, where the concentration of vacancies or density of dislocations are relatively high. As a proof of principle, we find that a high vacancy concentration stabilizes a defected ω -like phase in Nb which we will call the ω^* phase [39]. A vacancy-segregated region forms a stable interface with the bcc phase on the $[112]_{\text{bcc}}$ plane, as shown in Figs. S4 and S5. It needs dedicated DFT studies to fully understand the ω -phase transition in Nb, and details on the ω (and ω^*) phase and its structure are available in the Supplemental Material [40].

Finally, we consider the effects of the bcc-to- ω phase transition on the superconducting properties of Nb. As the ω -Nb displays a different electronic structure and electron-phonon coupling values compared to bcc Nb, it is anticipated that the superconducting properties, such as superconducting gap (Δ) and critical temperature (T_c), also differ in ω -Nb compared to bcc Nb [41–44]. For instance, there has been a report that the presence of substantial volume fractions of omega phase (≈ 5 vol.% according to TEM micrographs) leads to a change of T_c from 10.2 K to 6.8 K in Zr-15at.%Nb alloys [24]. Also, Ti-4.5at.%Mo and Ti-10at.%Mo alloys show that the formation of omega phase in Ti-Mo alloys degrades T_c [45].

To estimate T_c for the ω phase in Nb, we first consider the effect of the $\{111\}$ plane collapse on the Fermi-level density of states $N(0)$ which, to first approximation, is proportional to the electron-phonon coupling strength [42]. Interestingly, we find that even small displacements of the atoms away from their ideal bcc locations have a significant effect on the electronic structure and on the predicted T_c value, as shown in Fig. 4. We note that the reaction coordinate represents the transition state between bcc and ω -Nb associated with atomic shuffle of Nb atoms on the $\{112\}$ plane to the $\langle 111 \rangle$ direction. We also consider the ω^* phase; because this is a dynamically stable structure we can perform a more rigorous electron-phonon T_c calculation. This calculation yields a T_c of 1.1 K, similar to the value we would expect from its lower $N(0)$ relative to the bcc phase. The details of this calculation are available in the Supplemental Material [40,46,47]. With this evidence, we conclude that any ω -like phase will likely have significantly reduced T_c value, regardless of its precise microscopic structure.

Our findings suggest the ω phase regions could potentially lead to increased Cooper pair breaking and serve as a source

TABLE I. Vacancy formation energies in Nb.

Phase	Sites	Formation energy (eV)
bcc		2.77
ω	$(0001)_{\omega}$ plane A	1.22
ω	$(0001)_{\omega}$ plane B	-0.73

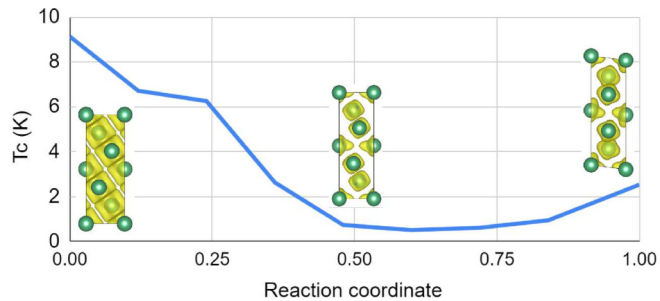


FIG. 4. Calculated effect of the bcc-to- ω phase transition on T_c . Inset figures illustrate the changing crystal structures as well as real space Fermi-level density of states contours in yellow.

of decoherence in superconducting qubit systems. It can cause the excitation of quasiparticles and degradation of quality factors of Nb resonators, and in turn, a decrease in T_1 of superconducting qubits, which may need a dedicated study to understand better. Additionally, the existence of ω -Nb phase in Nb thin films also indicates that this phase is possibly present in Nb thin films for superconducting radiofrequency (SRF) cavities for accelerator applications. As the size of the ω -Nb phase is 10–100 nm in this geometry, which again is comparable to the coherence length of Nb (≈ 40 nm), local deviations in superconducting properties can allow for magnetic flux penetration into Nb thin film SRF cavities and lead to a degradation in the overall quality factor [48,49]. While we observe the ω -phase formation in these samples, we do not observe the ω phase in epitaxially grown single-grain Nb thin film on sapphire (0001) substrates [27]. These observations suggest that by engineering the stresses at the metal/substrate interface and the density of crystalline defects and grain boundaries inherent to the Nb thin films, we can potentially mitigate the formation of this phase. A more detailed investigation aimed at linking film growth conditions to internal film stress as well as the formation of this phase is currently underway.

We report the discovery of omega (ω) phase in Nb thin films deposited by high-power impulse magnetron sputtering (HiPIMS) for superconducting qubits. XRD and TEM

analyses of Nb thin films indicates that internal stresses in the Nb thin films lead to $\{112\}\langle 111 \rangle$ deformation twinning of some Nb grains in the Nb thin films and the ω -phase are nucleated at the twin boundaries. Density functional theory (DFT) studies suggest that vacancies and dislocations can possibly play roles in stabilizing the ω phase at the twin boundaries in the Nb thin films. DFT studies also indicates that density of state (DOS) at Fermi level decrease in the ω phase and, in turn, the superconducting properties of ω -Nb may have suppressed T_c . It implies that such secondary phases can potentially introduce quantum decoherence in superconducting qubits through pairbreaking. We also note that the presence of this ω -phase transition in Nb may potentially matter for the Nb thin film superconducting radiofrequency (SRF) cavities, where they could allow for flux penetration and potentially lead to degradation in the quality factor.

We thank Dr. Sam Posen, Dr. Grigory V. Eremeev, and Dr. Martina Martinello for valuable discussions. We also thank Dr. S. kewalramani and Dr. K. V. L. V. Narayanachari for discussions on the analysis of stresses in Nb thin films using x-ray diffraction. This material is based upon work supported by the U.S. Department of Energy, Office of Science, National Quantum Information Science Research Centers, and Superconducting Quantum Materials and Systems Center (SQMS) under Contract No. DE-AC02-07CH11359, as well as the U.S. National Science Foundation under Award No. PHY-1549132, the Center for Bright Beams. We thank the Rigetti chip design and fabrication teams for the development and manufacturing of the qubit devices used in the reported experimental study, and for Rigetti Computing supporting the development of these devices. This work made use of the EPIC facility of Northwestern University's NUANCE Center, which has received support from the SHyNE Resource (NSF ECCS-2025633), the IIN, and Northwestern's MRSEC program (NSF DMR-1720139). Also, this work made use of the Jerome B. Cohen X-Ray Diffraction Facility supported by the MRSEC program of the National Science Foundation (DMR-1720139) at the Materials Research Center of Northwestern University and the Soft and Hybrid Nanotechnology Experimental (SHyNE) Resource (NSF ECCS-2025633).

-
- [1] C. R. H. McRae, H. Wang, J. Gao, M. R. Vissers, T. Brecht, A. Dunsworth, D. P. Pappas, and J. Mutus, Materials loss measurements using superconducting microwave resonators, *Rev. Sci. Instrum.* **91**, 091101 (2020).
- [2] A. Romanenko and D. Schuster, Understanding Quality Factor Degradation in Superconducting Niobium Cavities at Low Microwave Field Amplitudes, *Phys. Rev. Lett.* **119**, 264801 (2017).
- [3] A. Murthy, J. Lee, C. Kopas, M. Reagor, A. McFadden, D. Pappas, M. Checchin, A. Grassellino, and A. Romanenko, ToF-SiMS analysis of decoherence sources in superconducting qubits, *Appl. Phys. Lett.* **120**, 044002 (2022).
- [4] N. P. de Leon, K. M. Itoh, D. Kim, K. K. Mehta, T. E. Northup, H. Paik, B. Palmer, N. Samarth, S. Sangtawesin, and D. Steuerman, Materials challenges and opportunities for quantum computing hardware, *Science* **372**, eabb2823 (2021).
- [5] A. P. Place, L. V. Rodgers, P. Mundada, B. M. Smitham, M. Fitzpatrick, Z. Leng, A. Premkumar, J. Bryon, A. Vrajitoarea, S. Sussman *et al.*, New material platform for superconducting transmon qubits with coherence times exceeding 0.3 milliseconds, *Nat. Commun.* **12**, 1 (2021).
- [6] C. E. Murray, Material matters in superconducting qubits, *Mater. Sci. Engin.: R: Rep.* **146**, 100646 (2021).
- [7] M. V. P. Altoé, A. Banerjee, C. Berk, A. Hajr, A. Schwartzberg, C. Song, M. Alghadeer, S. Aloni, M. J. Elowson, J. M. Kreikebaum *et al.*, Localization and mitigation of loss in niobium superconducting circuits, *PRX Quantum* **3**, 020312 (2022).

- [8] A. Premkumar, C. Weiland, S. Hwang, B. Jäck, A. P. Place, I. Waluyo, A. Hunt, V. Bisogni, J. Pellicciari, A. Barbour *et al.*, Microscopic relaxation channels in materials for superconducting qubits, *Commun. Mater.* **2**, 72 (2021).
- [9] C. T. Earnest, J. H. Béjanin, T. G. McConkey, E. A. Peters, A. Korinek, H. Yuan, and M. Mariani, Substrate surface engineering for high-quality silicon/aluminum superconducting resonators, *Supercond. Sci. Technol.* **31**, 125013 (2018).
- [10] A. Megrant, C. Neill, R. Barends, B. Chiaro, Y. Chen, L. Feigl, J. Kelly, E. Lucero, M. Mariani, P. J. O'Malley *et al.*, Planar superconducting resonators with internal quality factors above one million, *Appl. Phys. Lett.* **100**, 113510 (2012).
- [11] J. Wenner, R. Barends, R. Bialczak, Y. Chen, J. Kelly, E. Lucero, M. Mariani, A. Megrant, P. O'Malley, D. Sank *et al.*, Surface loss simulations of superconducting coplanar waveguide resonators, *Appl. Phys. Lett.* **99**, 113513 (2011).
- [12] C. Müller, J. H. Cole, and J. Lisenfeld, Towards understanding two-level-systems in amorphous solids: Insights from quantum circuits, *Rep. Prog. Phys.* **82**, 124501 (2019).
- [13] D. P. Pappas, M. R. Vissers, D. S. Wisbey, J. S. Kline, and J. Gao, Two level system loss in superconducting microwave resonators, *IEEE Trans. Appl. Supercond.* **21**, 871 (2011).
- [14] A. A. Murthy, P. Masih Das, S. M. Ribet, C. Kopas, J. Lee, M. J. Reagor, L. Zhou, M. J. Kramer, M. C. Hersam, M. Checchin *et al.*, Developing a chemical and structural understanding of the surface oxide in a niobium superconducting qubit, *ACS Nano*. **16**, 17257 (2022).
- [15] J. Lee, Z. Sung, A. A. Murthy, M. Reagor, A. Grassellino, and A. Romanenko, Discovery of Nb hydride precipitates in superconducting qubits, [arXiv:2108.10385](https://arxiv.org/abs/2108.10385).
- [16] H. Xing and J. Sun, Mechanical twinning and omega transition by $\langle 111 \rangle \{112\}$ shear in a metastable β titanium alloy, *Appl. Phys. Lett.* **93**, 031908 (2008).
- [17] L. Hsiung and D. Lassila, Shock-induced deformation twinning and omega transformation in tantalum and tantalum-tungsten alloys, *Acta Mater.* **48**, 4851 (2000).
- [18] S. Sikka, Y. Vohra, and R. Chidambaram, Omega phase in materials, *Prog. Mater. Sci.* **27**, 245 (1982).
- [19] X. Li, Q. Zhao, Q. Wang, Y. Tian, H. Zhou, and J. Wang, Shear band mediated ω phase transformation in Nb single crystals deformed at 77 K, *Mater. Res. Lett.* **9**, 523 (2021).
- [20] X. Li, Q. Zhao, Y. Tian, Q. Wang, J. Fan, K. Song, H. Zhou, and J. Wang, Phase transformation induced transitional twin boundary in body-centered cubic metals, *Acta Mater.* **249**, 118815 (2023).
- [21] T. Bieler, N. Wright, F. Pourboghrat, C. Compton, K. Hartwig, D. Baars, A. Zamiri, S. Chandrasekaran, P. Darbandi, H. Jiang *et al.*, Physical and mechanical metallurgy of high purity Nb for accelerator cavities, *Phys. Rev. Spec. Top.—Accel. Beams* **13**, 031002 (2010).
- [22] J. Chakraborty, K. Kumar, R. Ranjan, S. G. Chowdhury, and S. Singh, Thickness-dependent fcc–hcp phase transformation in polycrystalline titanium thin films, *Acta Mater.* **59**, 2615 (2011).
- [23] B. M. Clemens and R. Sinclair, Metastable phase formation in thin films and multilayers, *MRS Bull.* **15**, 19 (1990).
- [24] S. Narasimhan, R. Taggart, and D. Polonis, The superconducting transition behavior of Zr-Nb binary alloys, *J. Nucl. Mater.* **43**, 258 (1972).
- [25] M. Murakami and T. Yogi, Strain in evaporated Nb thin films, *J. Appl. Phys.* **57**, 211 (1985).
- [26] B. Okolo, P. Lamparter, U. Welzel, and E. Mittemeijer, Stress, texture, and microstructure in niobium thin films sputter deposited onto amorphous substrates, *J. Appl. Phys.* **95**, 466 (2004).
- [27] S. Zhu, F. Crisa, M. Bal, A. Murthy, J. Lee, Z. Sung, A. Lunin, D. Frolov, R. Pilipenko, D. Bafia *et al.*, High quality superconducting Nb co-planar resonators on sapphire substrate, [arXiv:2207.13024](https://arxiv.org/abs/2207.13024).
- [28] S. Bose, P. Raychaudhuri, R. Banerjee, and P. Ayyub, Upper critical field in nanostructured Nb: Competing effects of the reduction in density of states and the mean free path, *Phys. Rev. B* **74**, 224502 (2006).
- [29] S. L. Sass, The structure and decomposition of Zr and Ti bcc solid solutions, *J. Less-Common Met.* **28**, 157 (1972).
- [30] D. Hoffman and J. A. Thornton, The compressive stress transition in Al, V, Zr, Nb, and W metal films sputtered at low working pressures, *Thin Solid Films* **45**, 387 (1977).
- [31] M. Hála, J. Čapek, O. Zabeida, J. Klemberg-Sapieha, and L. Martinu, Pulse management in high power pulsed magnetron sputtering of niobium, *Surf. Coat. Technol.* **206**, 4186 (2012).
- [32] C. Antoine, M. Foley, and N. Dhanaraj, *Physical Properties of Niobium and Specifications for Fabrication of Superconducting Cavities*, Tech. Rep. (Fermi National Accelerator Lab. (FNAL), Batavia, IL (United States), 2011).
- [33] R. Sundararaman, K. Letchworth-Weaver, K. A. Schwarz, D. Gunceler, Y. Ozhables, and T. A. Arias, JDFTx: Software for joint density-functional theory, *SoftwareX* **6**, 278 (2017).
- [34] J. P. Perdew, K. Burke, and M. Ernzerhof, Generalized Gradient Approximation Made Simple, *Phys. Rev. Lett.* **77**, 3865 (1996).
- [35] K. F. Garrity, J. W. Bennett, K. M. Rabe, and D. Vanderbilt, Pseudopotentials for high-throughput DFT calculations, *Comput. Mater. Sci.* **81**, 446 (2014).
- [36] I. Schnell and R. Albers, Zirconium under pressure: phase transitions and thermodynamics, *J. Phys.: Condens. Matter* **18**, 1483 (2006).
- [37] V. Popov, M. Stupak, and M. Urazaliev, Atomistic simulation of grain boundaries in niobium: Structure, energy, point defects and grain-boundary self-diffusion, *J. Phase Equilib. Diffus.* **43**, 401 (2022).
- [38] R. Hennig, T. Lenosky, D. Trinkle, S. Rudin, and J. Wilkins, Classical potential describes martensitic phase transformations between the α , β , and ω titanium phases, *Phys. Rev. B* **78**, 054121 (2008).
- [39] N. S. Sitaraman, Theory work on SRF materials, ProQuest dissertations and theses, 2022.
- [40] See Supplemental Material at <http://link.aps.org/supplemental/10.1103/PhysRevMaterials.7.L063201> for omega (ω) phase at Nb/Si interfaces (Fig. S1), orientation relationships at Nb/Si interface (Fig. S2), transport measurements (Fig. S3), and further detailed information on ω^* phase, which is ω -phase with 8 at.% of vacancies (Figs. S4-S5, and Table S1).
- [41] S. Y. Savrasov and D. Y. Savrasov, Electron-phonon interactions and related physical properties of metals from linear-response theory, *Phys. Rev. B* **54**, 16487 (1996).
- [42] W. McMillan, Transition temperature of strong-coupled superconductors, *Phys. Rev.* **167**, 331 (1968).
- [43] M. Sasaki, M. Koyano, H. Negishi, and M. Inoue, Fcc niobium films grown by halide chemical vapour deposition on ultrasound-vibrating substrates, *Thin Solid Films* **158**, 123 (1988).

- [44] J.-S. Oh, X. Fang, T.-H. Kim, M. Lynn, M. Kramer, M. Zarea, J. A. Sauls, A. Romanenko, S. Posen, A. Grassellino *et al.*, Multi-modal electron microscopy study on decoherence sources and their stability in Nb based superconducting qubit, [arXiv:2204.06041](https://arxiv.org/abs/2204.06041).
- [45] J. Ho and E. Collings, The influence of ω -phase on the superconductivity of Ti-Mo alloys, *Phys. Lett. A* **29**, 206 (1969).
- [46] P. B. Allen and R. C. Dynes, Transition temperature of strong-coupled superconductors reanalyzed, *Phys. Rev. B* **12**, 905 (1975).
- [47] J. Bekaert, A. Aperis, B. Partoens, P. M. Oppeneer, and M. V. Milošević, Advanced first-principles theory of superconductivity including both lattice vibrations and spin fluctuations: The case of FeB₄, *Phys. Rev. B* **97**, 014503 (2018).
- [48] J. Carlson, A. Pack, M. K. Transtrum, J. Lee, D. N. Seidman, D. B. Liarte, N. S. Sitaraman, A. Senanian, M. M. Kelley, J. P. Sethna *et al.*, Analysis of magnetic vortex dissipation in Sn-segregated boundaries in Nb₃ Sn superconducting RF cavities, *Phys. Rev. B* **103**, 024516 (2021).
- [49] A. R. Pack, J. Carlson, S. Wadsworth, and M. K. Transtrum, Vortex nucleation in superconductors within time-dependent Ginzburg-Landau theory in two and three dimensions: Role of surface defects and material inhomogeneities, *Phys. Rev. B* **101**, 144504 (2020).